

# Neonatal Irradiation Leads to Persistent Proteome Alterations Involved in Synaptic Plasticity in the Mouse Hippocampus and Cortex

Stefan J. Kempf,<sup>†,||</sup> Sara Sepe,<sup>†</sup> Christine von Toerne,<sup>‡</sup> Dirk Janik,<sup>§</sup> Frauke Neff,<sup>§</sup> Stefanie M. Hauck,<sup>‡</sup> Michael J. Atkinson,<sup>†,¶</sup> Pier G. Mastroberardino,<sup>†</sup> and Soile Tapiola\*,<sup>†,†</sup>

<sup>†</sup>Institute of Radiation Biology, <sup>‡</sup>Research Unit Protein Science, and <sup>§</sup>Institute of Pathology, Helmholtz Zentrum München, German Research Center for Environmental Health GmbH, 85764 Neuherberg, Germany

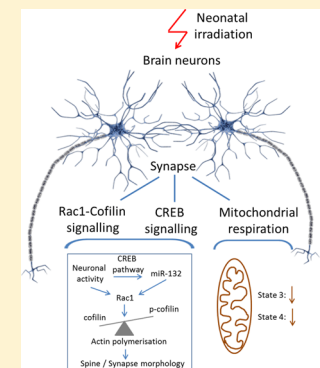
<sup>†</sup>Department of Genetics, Erasmus Medical Center, 3015 CE Rotterdam, The Netherlands

<sup>¶</sup>Chair of Radiation Biology, Technical University Munich, 80333 Munich, Germany

## Supporting Information

**ABSTRACT:** Recent epidemiological data indicate that radiation doses as low as those used in computer tomography may result in long-term neurocognitive side effects. The aim of this study was to elucidate long-term molecular alterations related to memory formation in the brain after low and moderate doses of  $\gamma$  radiation. Female C57BL/6J mice were irradiated on postnatal day 10 with total body doses of 0.1, 0.5, or 2.0 Gy; the control group was sham-irradiated. The proteome analysis of hippocampus, cortex, and synaptosomes isolated from these brain regions indicated changes in ephrin-related, RhoGDI, and axonal guidance signaling. Immunoblotting and miRNA-quantification demonstrated an imbalance in the synapse morphology-related Rac1-Cofilin pathway and long-term potentiation-related cAMP response element-binding protein (CREB) signaling. Proteome profiling also showed impaired oxidative phosphorylation, especially in the synaptic mitochondria. This was accompanied by an early (4 weeks) reduction of mitochondrial respiration capacity in the hippocampus. Although the respiratory capacity was restored by 24 weeks, the number of deregulated mitochondrial complex proteins was increased at this time. All observed changes were significant at doses of 0.5 and 2.0 Gy but not at 0.1 Gy. This study strongly suggests that ionizing radiation at the neonatal state triggers persistent proteomic alterations associated with synaptic impairment.

**KEYWORDS:** ionizing radiation, brain, mitochondria, synapse, proteomics, cerebellum, miR-132, Rac1, dendritic spine, memory



## INTRODUCTION

Human exposure to ionizing radiation is increasing in the developed world, primarily due to frequent usage in medical imaging.<sup>1</sup> The damaging effect of high doses of ionizing radiation on hippocampal neurogenesis and functioning such as cognition is well-known.<sup>2</sup> Radiation-associated impairment in learning and memory is observed in the clinical setting after high-dose brain radiation therapy.<sup>3</sup> However, epidemiological data suggest that doses considerably lower than those used in radiotherapy may also lead to cognitive impairment such as memory and learning deficits, especially in the young.<sup>4–6</sup> There is still considerable uncertainty regarding the mechanisms underlying these effects.

Children with minor traumatic brain injuries commonly undergo multiple imaging procedures where single radiation doses lie close to 0.01 Gy.<sup>7</sup> More than 1.5 million children are screened with CT scans yearly in the Western hemisphere.<sup>8</sup> Infants and children may represent a group with especially high radiation sensitivity for several reasons. On the one hand, at this developmental stage, the brain is immature and rapidly developing. On the other hand, their long future life expectancy

allows injuries with prolonged latencies to develop. Therefore, an improved understanding of the biological mechanisms of radiation-induced impairment in memory and learning is essential for preventive purposes.

During the early phases of childhood, the volume of gray matter in the central nervous system (CNS) increases rapidly, peaking at around four years of age.<sup>9</sup> This specific phase of rapid brain maturation, the brain growth spurt,<sup>10</sup> involves phases of axonal and dendritic growth including the establishment and remodelling of neuronal circuits.<sup>11,12</sup> In rodents, the corresponding time window of the brain growth spurt spans the second and fourth postnatal week.<sup>13</sup> It has been shown that toxic agents administered to neonatal mice within this window of susceptibility can lead to disruption of adult brain function<sup>14</sup> and can be intensified by exposure to low-dose ionizing radiation on postnatal day 10 (PND10).<sup>15</sup> At this specific stage, exposure to ionizing radiation alone leads to long-term neurocognitive deficits characterized by proinflammatory

Received: June 18, 2015

Published: September 29, 2015

changes, reflected in an increased number of activated microglia.<sup>16,17</sup> Proinflammatory factors produced by the activated microglia include IL-6, TNF- $\alpha$ , reactive oxygen species, and nitric oxide, all of which have been shown to suppress mitochondrial function.<sup>18</sup> Accruing data support a causal association between this early radiation exposure and long-term mitochondrial impairment in the brain.<sup>19,20</sup> As mitochondria are concentrated in synapses,<sup>21</sup> radiation-induced changes in synaptic morphology may affect mitochondrial structure and function in this compartment.<sup>22,23</sup>

We have previously shown that neonatally irradiated NMRI male mice show persistent alterations in synaptic plasticity, adult neurogenesis, and neuroinflammation after a dose of 1.0 Gy. Cognition was significantly impaired already at a dose of 0.5 Gy.<sup>17</sup> In the present study, we used female C57BL/6J mice to investigate the strain and gender specificity of the radiation effects. We also included exposure to a much lower dose, comparable to a cumulative dose after a few CT scans (0.1 Gy). Hippocampus, cortex, and isolated synaptosomes were analyzed using global proteomics, immunoblotting, pathway-focused transcriptomics, miRNA quantification, and *ex vivo* mitochondrial respiration. In addition, the radiation-induced proteome alterations in the cerebellum were investigated. Ionizing radiation induced significant changes in the Rac1-Cofilin and cAMP response element-binding protein (CREB) signaling pathways. A significant reduction in hippocampal mitochondrial respiration capacity was observed in young (4/5 weeks) but not in mature (24 weeks) mice. However, marked alterations in the expression of proteins involved in mitochondrial function and synaptic plasticity remained present in aged mice after doses of 0.5 and 2.0 Gy but were not detectable at lower doses.

## MATERIALS AND METHODS

### Ethical Statement, Irradiation of Animals, and Whole Tissue Collection

Experiments were carried out according to protocol number 139–12–30 approved by animal experiments committee DEC-consult of The Netherlands (EMC number 3018). Female C57BL/6J mice were total body irradiated on PND10 with a single exposure of gamma irradiation (<sup>137</sup>Cs, 0.082 Gy/min) at doses of 0 (sham), 0.1, 0.5, and 2.0 Gy (Erasmus University Medical Centre EDC, The Netherlands). The radiation field was homogeneous within  $\pm 3\%$  as verified by a TLD-100 dosimeter. Three litters were used within each irradiation group to minimize interlitter effects; neonates from each litter were irradiated together. Animals were shipped to Helmholtz Zentrum München, Germany, 1–2 weeks postirradiation and kept under standard housing conditions until their experimental usage.

Mice were sacrificed via cervical dislocation after either 4–5 weeks or 6 months. Brains were excised and transferred to ice-cold phosphate-buffered saline (PBS), rinsed carefully, and dissected under stereomicroscopic inspection while maintaining cold conditions. Hippocampi, cortices without meninges, and cerebella from each hemisphere were separately sampled, gently rinsed in ice-cold PBS, and snap-frozen in liquid nitrogen for whole tissue analysis. For the isolation of intact synaptosomes and total mitochondria, brain regions were maintained chilled but not frozen until the final isolation procedure.

### Isolation and Enrichment of Synaptosomes for Proteomics Analysis

Isolation and enrichment of synaptosomes were performed in accordance with the protocol of Kiebisch et al.<sup>24</sup> with slight modifications. Briefly, isolated hippocampi, cortices, and cerebella were transferred to a precooled glass tissue grinder of dounce type (#357538, Wheaton). Tissues were homogenized in isolation buffer (IB) (0.32 M sucrose, 10 mM Tris-HCl, 1 mM EDTA-K, pH 7.4) using eight strokes with a “loose” and eight strokes with a “tight” pestle. All preparation steps were done on ice. The homogenates were centrifuged (4 °C, 1000g, 5 min), and the supernatant containing synaptosomes/nonsynaptosomal mitochondria was collected, whereas the pellet was washed twice with IB and centrifuged (4 °C, 1000g, 5 min), collecting each time the supernatants. Subsequently, the pooled supernatants were centrifuged again (4 °C, 1000g, 5 min) and transferred to fresh tubes. Supernatants were centrifuged (4 °C, 14 000g, 15 min) to pellet synaptosomes/nonsynaptosomal mitochondria. The pellets were resuspended in 3 mL of ice-cold IB and layered on a 7.5/12% discontinuous Ficoll gradient (4 °C) (FicollPM400, Sigma-Aldrich) to separate and purify synaptosomes from nonsynaptosomal mitochondria. The gradient was ultracentrifuged (4 °C, 73 000g, 36 min) (Ultracentrifuge Optima L70 with swing-out rotor, Beckman). The synaptosome layer was transferred to fresh tubes and resuspended in IB (1:3, v/v, final volume 2 mL). Purified synaptosomes were pelleted by centrifugation (4 °C, 16 000g, 15 min), and the pellets were washed with IB containing 0.5 mg/mL bovine serum albumin [(BSA), fatty-acid free]. Subsequently, the samples were centrifuged again (4 °C, 16 000g, 15 min) and washed with IB. Finally, synaptosomes were pelleted via centrifugation (4 °C, 16 000g, 15 min) and frozen (−20 °C) until further analysis.

### Evaluation of Synaptosome Intactness and Enrichment Quality by Mitochondrial Respiration and Immunoblotting Using Nonirradiated Animals

Evaluation of the intactness of mitochondria within the synaptosome fraction was investigated using mitochondrial respiration measurement from nonirradiated test animals following the protocol of Choi et al.<sup>25</sup> with slight modifications as described further in the *Isolation and Respiration Analysis of Total Hippocampal Mitochondria* section.

Immunoblots of 10  $\mu$ g subfractions were incubated with primary antibody dilutions as recommended by the manufacturer: COXIV subunit IV-MS407 (Mitoscience),  $\beta$ -Actin-sc-1616 (Santa Cruz), LSD1-2139 (Cell Signaling), PLP-sc-98781 (Santa Cruz), and SNAP-25-SMI-81R (Covance). Immunoblots were performed and analyzed as described further in the *Immunoblotting* section.

### Proteome Analysis

The analysis of proteome changes was done using the isotope coded protein label (ICPL) approach (SERVA Electrophoresis GmbH, Germany), as reported in detail previously.<sup>17</sup> Briefly, the whole tissue protein lysates (5  $\mu$ g in 5  $\mu$ L of 6 M guanidine hydrochloride) originating from six individual hippocampal, cortical, or cerebellar tissue replicates from either control or irradiated groups at 4 weeks and 24 weeks postirradiation were investigated. For synaptosomal protein analysis, three biological replicates consisting of pooled synaptosomes from two mice from either sham- or irradiated groups 5 weeks and 24 weeks postirradiation were used. All samples were reduced, alkylated, and labeled with ICPL reagents as follows: control with ICPL-

0, 0.1 Gy with ICPL-4, 0.5 Gy with ICPL-6, and 2.0 Gy samples with ICPL-10.

The labeled samples representing each radiation dose at one time point were combined, followed by one-dimensional protein separation with 12% SDS-PAGE (polyacrylamide gel electrophoresis), as described elsewhere.<sup>26</sup> The protein bands were visualized with Coomassie Blue, and the gel lanes were cut into five equal slices, destained, and trypsinised overnight, as described before.<sup>27</sup> Peptides were extracted and acidified with 1% formic acid followed by liquid chromatography–tandem mass spectrometry (LC–MS/MS) analysis on an LTQ-Orbitrap XL (Thermo Fisher) as described previously.<sup>26</sup>

For protein identification and quantification, MS–MS spectra were searched against the ENSEMBL mouse database (Version: 2.4, 56416 sequences) via MASCOT (version 2.3.02; Matrix Science) with a mass tolerance of 10 ppm for peptide precursors and 0.6 Da for MS–MS peptide fragments, including not more than one missed cleavage. Carbamidomethylation of cysteine and ICPL-0, ICPL-4, ICPL-6, and ICPL-10 for lysine was set as fixed modifications. The ICPL pairs analyzed by Proteome discoverer software (Version 1.3, Thermo Fisher) were used to identify and quantify the proteins. To ensure a confident global protein analysis, the percolator algorithm ( $p < 0.01$ ) and false discovery rate (FDR) criteria ( $\text{FDR} < 0.01$ ) were used as reported previously.<sup>17,26</sup> Proteins from each LC–MS run were normalized against the median of all quantifiable proteins and were considered significantly deregulated if they fulfilled the following criteria: (i) identification by at least two unique peptides in  $n - 1$  MS runs ( $n$ , number of biological replicates), (ii) quantification with an ICPL-variability of  $\leq 30\%$ , and (iii) a fold-change of  $\geq 1.3$  or  $\leq -1.3$ . The threshold of  $\pm 1.3$  is based on our average experimental technical variance of the multiple analysis of hippocampal and cortical technical replicates, as described in detail elsewhere.<sup>17</sup>

### Bioinformatics Analysis

Deregulated proteins were assigned to functional classes using PANTHER classification system software (<http://www.pantherdb.org>) and the general annotation from UniProt (<http://uniprot.org>). To identify radiation-affected signaling pathways, a core and comparison signaling pathway analysis was performed with all deregulated proteins from each dose group using INGENUITY pathway analysis (IPA) (<http://www.ingenuity.com>) applying databases of experimental and predictive origin. The IPA comparison analysis takes into account the signaling pathway rank according to the calculated  $p$ -value and reports it hierarchically. The software generates significance values ( $p$ -values) between each biological or molecular event and the imported proteins based on the Fischer's exact test ( $p \leq 0.05$ ).

### Data Deposition of Proteomics Experiments

The raw-files of the obtained MS–MS spectra can be found under [http://storedb.org/project\\_details.php?projectid=51](http://storedb.org/project_details.php?projectid=51) with the ProjectID 52.

### Isolation and Respiration Analysis of Total Hippocampal Mitochondria

Animals were killed by cervical dislocation, brains were rapidly excised on an ice-cold plate, and hippocampi were rapidly dissected. For mitochondrial extraction, hippocampi were minced in 10 volumes of mitochondrial isolation buffer (70 mM sucrose, 210 mM mannitol, 5 mM HEPES, 1 mM EGTA,

and 0.05% fatty acid free bovine serum albumin), pH 7.2, and the pieces were rinsed several times to remove all blood. The tissue was processed with a drill-driven Teflon dounce homogenizer, and the solution was centrifuged at 800g for 10 min at 4 °C, after which the supernatant was transferred in a clean tube and spun again (8000g, 10 min, 4 °C). The pellet was resuspended in mitochondrial isolation buffer and spun again. The final pellet was resuspended in a minimal volume of mitochondrial isolation buffer, and protein concentration was determined by standard Bradford assay. Respiration was measured with a XF-24 extracellular flux analyzer (Seahorse Bioscience). Ten micrograms of mitochondrial protein was loaded in each well of a Seahorse plate, which was then spun 2000g, 20 min, at 4 °C. Next, mitochondrial isolation buffer volume was adjusted to 450 μL per well, and the plate was incubated 8 min at 37 °C. Respiration was sustained by succinate (10 mM) in the presence of rotenone (4 μM). State 3 was elicited by addition of 8 mM ADP. The oxygen consumption rate (OCR) was assessed in response to Oligomycin (2.5 μg/mL), FCCP (4 μM), and Antimycin A (4 μM). Each experimental group included four animals.

### Immunoblotting

Protein extracts (10 μg) from whole hippocampus and cortex (24 weeks post-irradiation) were separated on 12% SDS polyacrylamide gels and transferred to nitrocellulose membranes (GE Healthcare) via BIO-RAD Criterion Blotter system, as described recently.<sup>26</sup> Blots were incubated with primary antibody dilutions (diluted in Roti<sup>R</sup>-Block solution) overnight at 4 °C as recommended by the manufacturer. Details of the used antibodies can be found in SI Table S10. The blots were developed using ECL system (GE Healthcare) using the standard protocol from the manufacturer. GAPDH was not significantly deregulated based on the global proteomics results in any sample and was therefore used as a loading control. Immunoblots were quantified with TotalLab TL100 software ([www.totallab.com](http://www.totallab.com)) using software-suggested background correction. Three biological replicates were used for statistical analysis (unpaired Student's  $t$  test) with a significance threshold of 0.05.

### Isolation of Total Protein and RNA from Frozen Brain Regions

Individual frozen hippocampi, cortices, and cerebella were homogenized with 6 M guanidine hydrochloride (SERVA Electrophoresis GmbH, Germany) on ice using a manual plastic mortar. Homogenates were briefly vortexed, sonicated, and cleared by centrifugation (20 000g, 1 h, 4 °C). The supernatants were collected and stored at –20 °C before further use. Total protein content was determined using the Bradford assay (Thermo Fisher) following the manufacturer's instructions.

Total RNA from individual frozen hippocampi and cortices was isolated and purified by mirVana Isolation Kit (Ambion) according to the manufacturer's instructions. Total RNA was eluted with nuclease-free water. The optical density (OD) ratio of 260/280 was measured using a Nanodrop spectrophotometer (PepLab Biotechnology; Germany); it ranged between 1.9 and 2.1. The eluates were stored at –20 °C until further analysis.

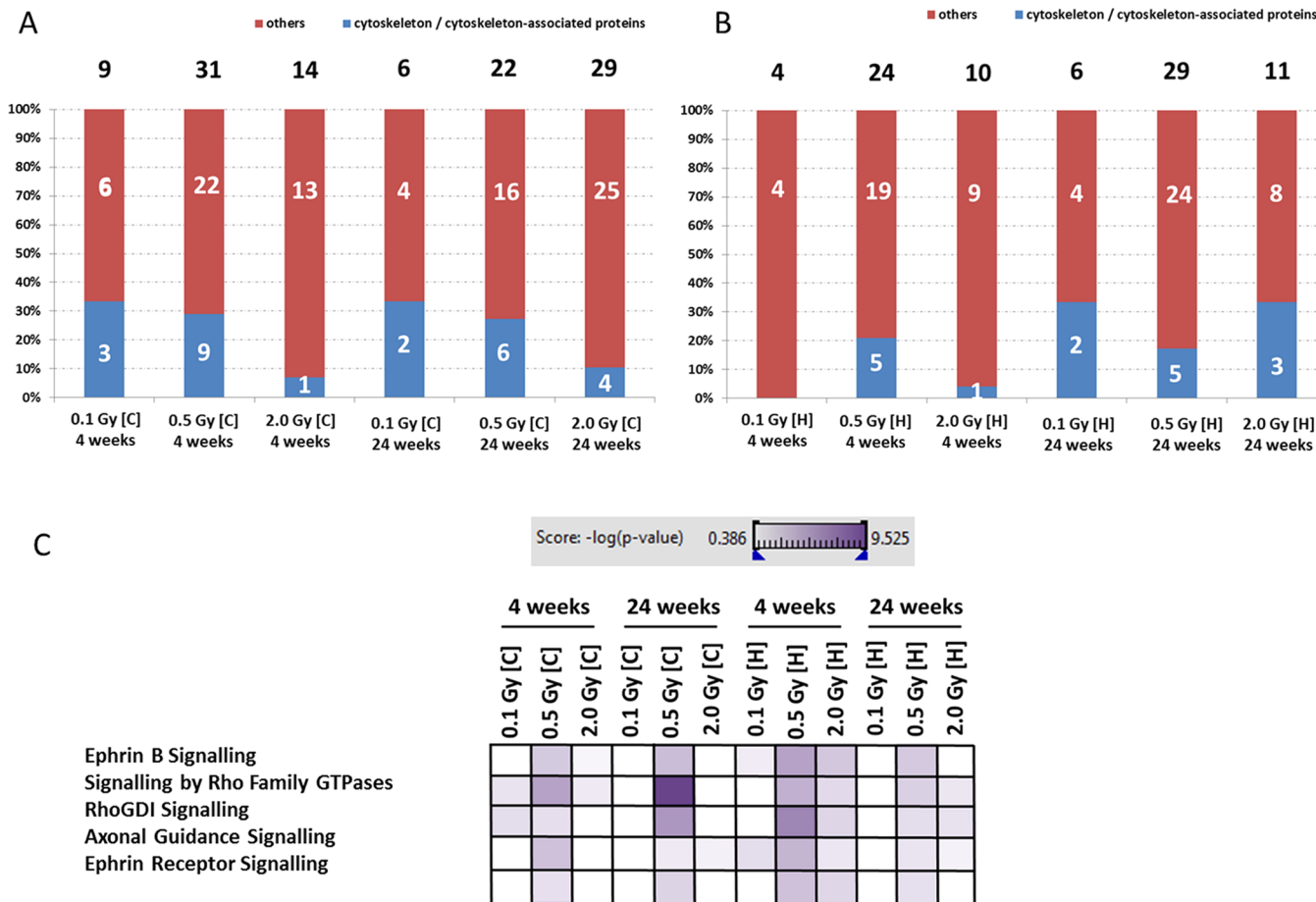


**Figure 1.** MS-based proteomics of whole mouse hippocampus and cortex at 4 weeks and 24 weeks postirradiation. Panels A and B show a comparison of the number of hippocampal and cortical deregulated proteins. The proteins were grouped into the protein class cytoskeleton/cytoskeleton-associated proteins and others to obtain information about the long-term radiation-induced alterations of protein classes and potential biological targets. The protein classification is based on information from the PANTHER software (PANTHER protein class) and UniProt database. The numbers within the columns represent the number of proteins involved in this protein class. The number above the columns represents the total number of deregulated proteins at this dose and brain region. Panel C shows the associated signaling pathways of all deregulated proteins using the IPA software tool. High color intensity represents high significance ( $p$ -value); all colored boxes have a  $p$ -value of  $\leq 0.05$ . C, Cortex; H, hippocampus; six individual biological replicates were used from cortex and hippocampus per dose group and time point.

#### Quantification of miRNAs miR-132 and miR-134 via Quantitative RT-PCR

RNA isolates of brain tissues (10 ng) from whole hippocampus and cortex (24 weeks postirradiation) were used to quantify miR-132 and miR-134 expression levels using the TaqMan Single MicroRNA Assay (Applied Biosystems) according to the manufacturer's protocol. Steps included a reverse transcription and real-time PCR (StepOnePlus) via Taqman-primers (mmu-miR-132 (ID000457), mmu-miR-134 (ID001186), snoRNA135 (ID001239), Life Technologies). Expression levels of miRNA were calculated based on the  $2^{-\Delta\Delta Ct}$  method with normalization against endogenous snoRNA135.<sup>28</sup> Changes were considered significant if they reached a  $p$ -value of  $\leq 0.05$  (unpaired Student's  $t$  test,  $n = 3$  per dose group).

#### Pathway-Focused Gene Expression Analysis

Sham- and 2.0 Gy-irradiated cortical RNA isolates (100 ng, 24 weeks postirradiation) were used to quantify the gene expression of 84 genes related to synaptic plasticity (RT2 Profiler Mouse Synaptic Plasticity, PAMM-126Z, Qiagen). The relative expression of genes was normalized against the median of all 84 target genes using the eq  $2^{-\Delta\Delta Ct}$ , where  $\Delta\Delta Ct = \Delta Ct_{\text{irradiated}} - \Delta Ct_{\text{sham}}$  and  $\Delta Ct = Ct_{\text{target-mRNA}} - Ct_{\text{median-of-84-target-genes}}$ . Three biological replicates were used within each group. Gene expression changes were considered to be significant if they reached a  $p$ -value of  $\leq 0.05$  and if they had a fold-change of  $\geq 1.2$  or  $\leq -1.2$ . The threshold of  $\pm 1.2$  was based on the average experimental technical variance (8.4%) and biological variance (6.9%) of a set of 14 overlapping target genes, as shown elsewhere.<sup>17</sup>

**Brain Morphology and Myelination Staining**

Formalin-fixed paraffin-embedded tissues were prepared using standard techniques.<sup>29</sup> For histology, 4  $\mu\text{m}$  thick sagittal whole brain sections were cut from paraffin blocks, dewaxed, and rehydrated. Subsequently, the slides were incubated with 0.1% Triton X in PBS for 30 min and washed with PBS. Klüver Barrera staining to determine demyelination processes (myelin and Nissl substances in neurons) was performed with incubation in luxol fast blue solution (L0294, Sigma-Aldrich) overnight at 60 °C. After a short washing in ethanol and water, the slides were incubated in 0.05% lithium carbonate solution (62470, Fluka) for a few seconds. The slides were destained in ethanol until the color became sky/light blue and washed again in water. The brain slides were counterstained with cresyl violet (Certustain, 105235, Merck), washed in water and ethanol, and

#### Brain Morphology and Myelination Staining

Formalin-fixed paraffin-embedded tissues were prepared using standard techniques.<sup>29</sup> For histology, 4  $\mu\text{m}$  thick sagittal whole brain sections were cut from paraffin blocks, dewaxed, and rehydrated. Subsequently, the slides were incubated with 0.1% Triton X in PBS for 30 min and washed with PBS. Klüver Barrera staining to determine demyelination processes (myelin and Nissl substances in neurons) was performed with incubation in luxol fast blue solution (L0294, Sigma-Aldrich) overnight at 60 °C. After a short washing in ethanol and water, the slides were incubated in 0.05% lithium carbonate solution (62470, Fluka) for a few seconds. The slides were destained in ethanol until the color became sky/light blue and washed again in water. The brain slides were counterstained with cresyl violet (Certustain, 105235, Merck), washed in water and ethanol, and

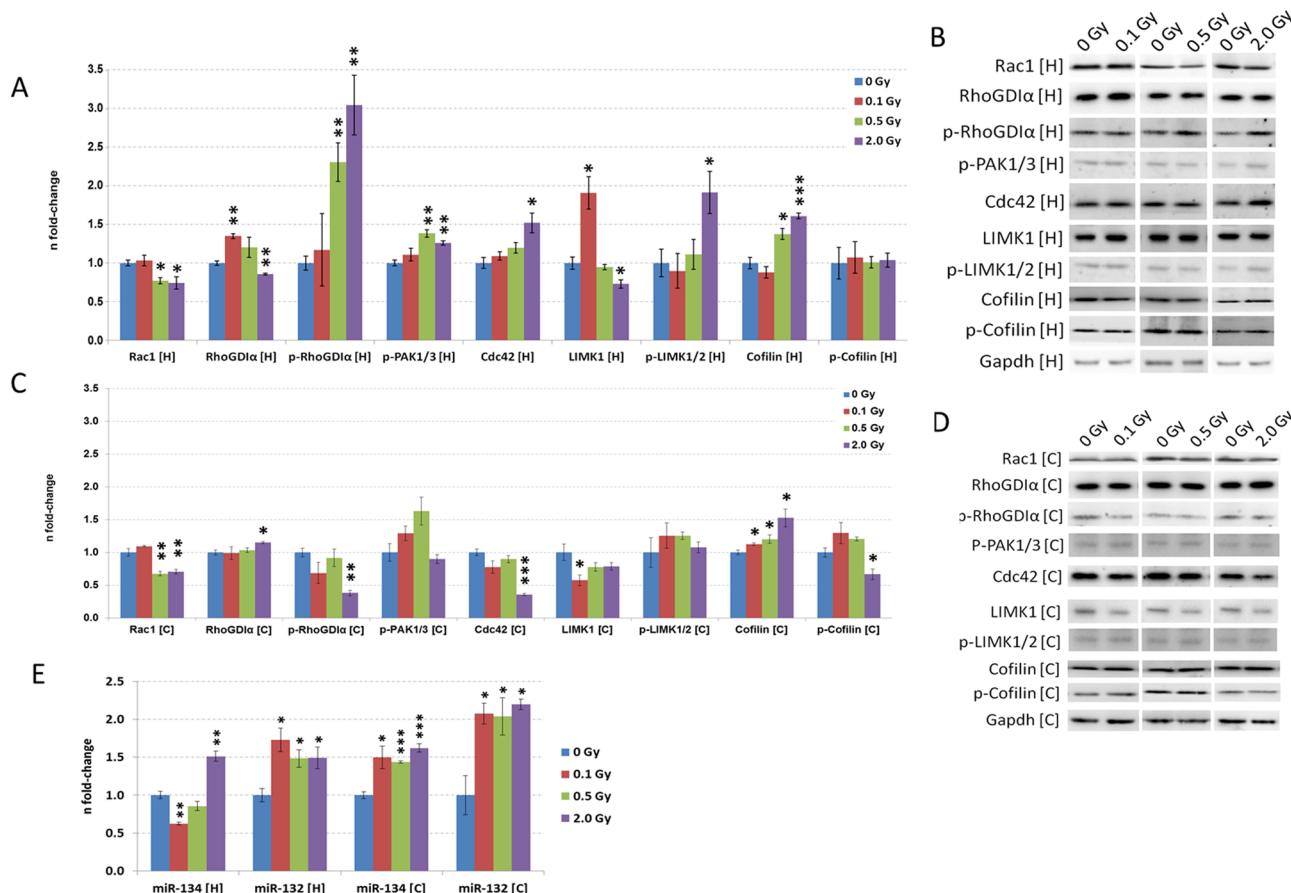


**Figure 2.** Immunoblotting and miRNA quantification of the Rac1-Cofilin signaling pathway. Data are shown from (A–D) immunoblotting and (E) miRNA quantification of members of the Rac1-Cofilin pathway in hippocampus (data are depicted in panels A, B, and E) and cortex (data are depicted in panels C, D, and E) irradiated with 0 Gy, 0.1 Gy, 0.5 Gy, and 2.0 Gy 24 weeks postirradiation. The columns represent the fold-changes with standard errors of the mean (SEM);  $n = 3$ . \*,  $p < 0.05$ ; \*\*,  $p < 0.01$ ; \*\*\*,  $p < 0.001$  (unpaired Student's *t* test). Normalization was performed against endogenous GAPDH and endogenous snoRNA135 for immunoblotting and miRNA quantification, respectively. H, hippocampus; C, cortex.

were coverslipped for light microscopy analysis. The slides were scanned with a Hamamatsu NanoZoomer. To evaluate global changes in brain morphology, the brain slides were stained with hematoxylin/eosin (Mayer's hematoxylin, M0602, Bio-Optica and eosin Y 1% aqueous solution, 05–10002/L, Bio-Optica) after standard procedures.

## RESULTS

### Ionizing Radiation Affects Cytoskeleton and Cytoskeleton-Associated Proteins

Global quantitative proteome analysis using LC–MS was performed to quantify alterations in the hippocampus and cortex 4 and 24 weeks postirradiation. The complete list of deregulated proteins is shown in SI Tables S1 (cortex) and S2 (hippocampus). The protein quantification showed that the number of deregulated proteins was lower at 0.1 Gy than at higher doses at 4 weeks (cortex/hippocampus: 0.1 Gy, 9/4 proteins; 0.5 Gy, 31/24 proteins; 2.0 Gy, 14/10 proteins) and at 24 weeks (cortex/hippocampus: 0.1 Gy, 6/6 proteins; 0.5 Gy, 22/29 proteins; 2.0 Gy, 29/11 proteins) (Figure 1A,B). That is also reflected in the ratio of affected proteins to all quantifiable proteins ( $\geq 2$  unique ICPL-labeled peptides found in  $n - 1$  runs) at 4 weeks (cortex/hippocampus: 0.1 Gy, 1.7%/1.0%; 0.5 Gy, 5.8%/6.0%; 2.0 Gy, 2.6%/2.5%) and 24 weeks postirradiation (cortex/hippocampus: 0.1 Gy, 1.1%/1.6%; 0.5 Gy, 3.7%/4.0%; 2.0 Gy, 4.2%/2.1%). Several of the deregulated

proteins belonged to the functional group of cytoskeleton/cytoskeleton-associated proteins, especially at the dose of 0.5 Gy in cortex (4 weeks: 0.5 Gy, 29%; 2.0 Gy, 7% and 24 weeks: 0.5 Gy, 27%; 2.0 Gy, 10%) and in hippocampus (4 weeks: 0.5 Gy, 20%; 2.0 Gy, 4% and 24 weeks: 0.5 Gy, 17%; 2.0 Gy, 33%) (Figure 1A,B; SI Tables S1 and S2, PANTHER protein classes are highlighted in brown). The involved proteins were mostly related to actin/actin-associated signaling but also to tubulin/tubulin-associated signaling. Importantly, we observed an increase in a number of septin proteins (Sept3, 5, 7, 8, and 11) that organize the actin microfilaments. Further, we noted changes in the expression of several subunits of tubulin proteins (Tubb's) and neurofilament proteins (Nefh, Nefm) that are involved in the maintenance of the neuronal caliber and mature axons (SI Tables S1 and S2).

The bioinformatics analysis showed that the signaling by ephrin B/ephrin receptor, Rho family GTPases, and RhoGDI as well as axonal guidance signaling were all significantly altered, especially at the dose of 0.5 Gy (Figure 1C). These signaling pathways were not significantly changed 24 weeks after the dose of 0.1 Gy (Figure 1C).

All significantly altered pathways have common proteins such as the Rho family GTPase Rac, the kinases PAK and LIMK, and the actin cytoskeleton-remodelling protein cofilin. All these proteins are involved in axonal maturation, spine and synapse

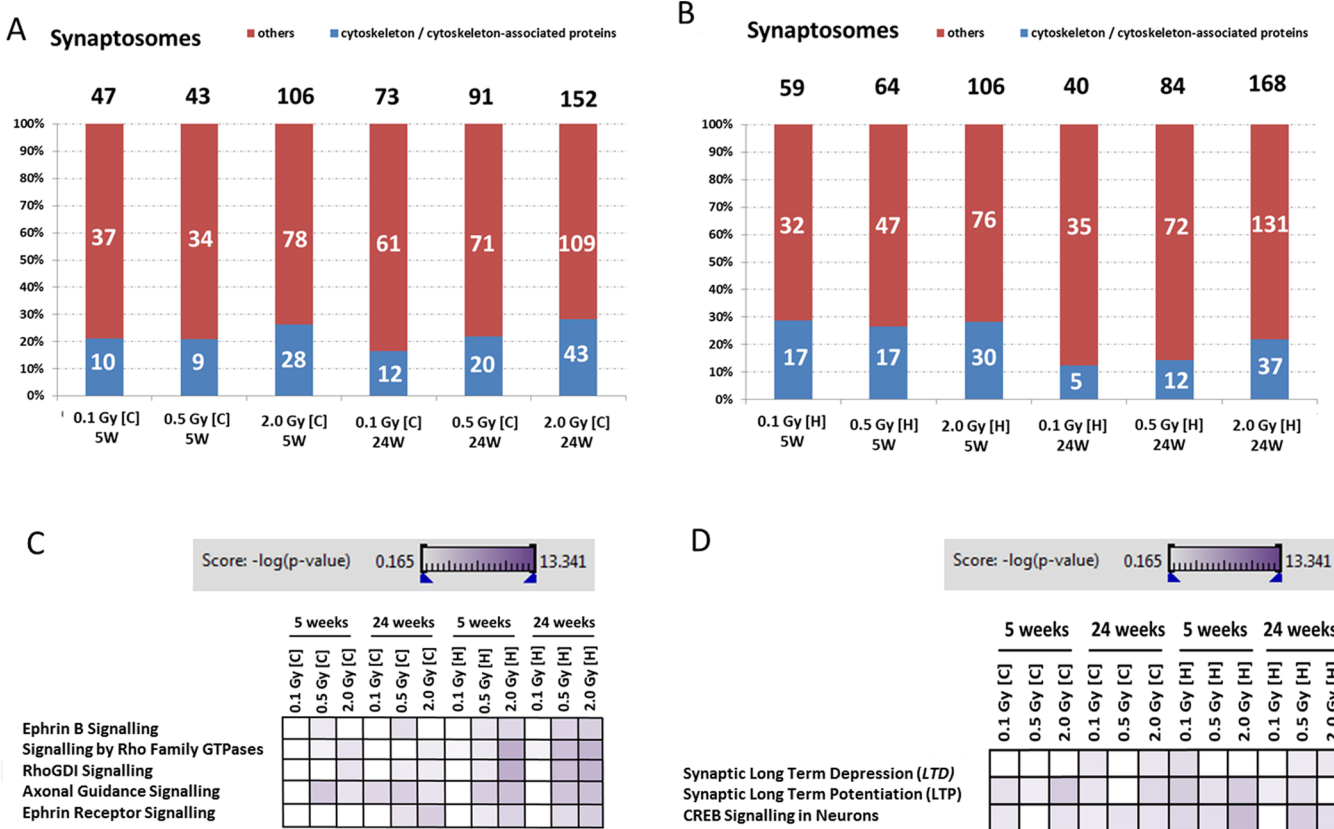


**Figure 3.** Proteomics analysis of hippocampal and cortical synaptosomes at 5 weeks and 24 weeks postirradiation. Panels A and B show a comparable representation of the number of hippocampal and cortical deregulated proteins in isolated synaptosomes. The proteins were grouped into the classes cytoskeleton/cytoskeleton-associated proteins and others to provide information about the long-term radiation-induced alterations of protein classes and potential biological targets. The protein classification is based on information from the PANTHER software (PANTHER protein class) and UniProt database. The numbers within the columns represent the number of proteins involved in this protein class. The number above the columns represents the total number of deregulated proteins at this dose and brain region. Panels C and D show the associated signaling pathways of all the deregulated proteins using the IPA software tool. High color intensity represents high significance (*p*-value); all colored boxes have a *p*-value of  $\leq 0.05$ . C, Cortex; H, hippocampus;  $n = 3$  per dose group, time point, and brain region, whereas each biological replicate corresponds to a pooled sample from two individual animals.

formation, maturation, and morphology via regulation of actin polymerization (Rac1-Cofilin pathway).<sup>30–32</sup>

#### Ionizing Radiation Impairs the Rac1-Cofilin Signaling Pathway

To validate the potential radiation-induced alterations in the Rac1-Cofilin pathway, immunoblotting and miRNA quantification of some key up- and downstream molecules of this pathway were performed. The analysis was done 24 weeks after radiation exposure to investigate the persistent changes.

We noted reduced Rac1 levels at 0.5 and 2.0 Gy but not at 0.1 Gy both in hippocampus and cortex (Figure 2A–D), correlating with proteomics data (hippocampus: 0.5 Gy, -1.31; 2.0 Gy, -1.39 and cortex: 0.5 Gy, -1.33; 2.0 Gy, -1.35) (SI Tables S1 and S2). For comparison, the proteomics data also showed reduced level of Rac1 at 4 weeks (hippocampus: 0.5 Gy, -1.36; 2.0 Gy, -1.31 and cortex: 0.5 Gy, -1.47; 2.0 Gy, -1.30) (SI Tables S1 and S2). In spite of the reduced expression of Rac1, the level of miR-132 that is able to indirectly increase Rac1 activity by blocking the GTPase-activating protein p250GAP<sup>33,34</sup> was enhanced at all doses in both brain regions (Figure 2E). Moreover, in hippocampus, the expression of phosphorylated forms of RhoGDI $\alpha$ , PAK1/3, and LIMK1/2 was markedly increased at 0.5 and 2.0 Gy (Figure 2A,B), also suggesting an activation of Rac1. The reverse

picture was observed in the cortex, as the phosphorylation status of RhoGDI $\alpha$  was decreased more than two-fold at 2.0 Gy (Figure 2C,D). Since miR-134 is suggested to negatively regulate the LIMK1 level,<sup>35</sup> its expression was tested (Figure 2A,B,E). In the hippocampus, the level of miR-134 inversely correlated to that of LIMK1 at all doses. In cortex, the increase in miR-134 expression inversely correlated with the significantly decreased expression of LIMK1 only at 0.1 Gy (Figure 2C–E). Finally, we observed an increase in total cofilin levels in the hippocampus (0.5 and 2.0 Gy) and cortex (all doses). The level of phosphorylated cofilin was altered only in cortex at 2.0 Gy where it was significantly reduced (Figure 2A–D). This suggests that the ratio of phospho- to total cofilin is altered by irradiation in favor of total cofilin, as has been observed in our previous studies of irradiated NMRI mice.<sup>17</sup>

#### Irradiation Persistently Affects Synaptic Plasticity in the Dendritic Spines of Neurons

To get more insight into the signaling pathways associated with synapses, neuronal synaptosomes were isolated from whole hippocampus and cortex at 5 weeks and 24 weeks postirradiation. The enrichment of synaptosomes and intactness of synaptosomal mitochondria was tested by immunoblotting and mitochondrial respiratory capacity, respectively (SI Figure S1).

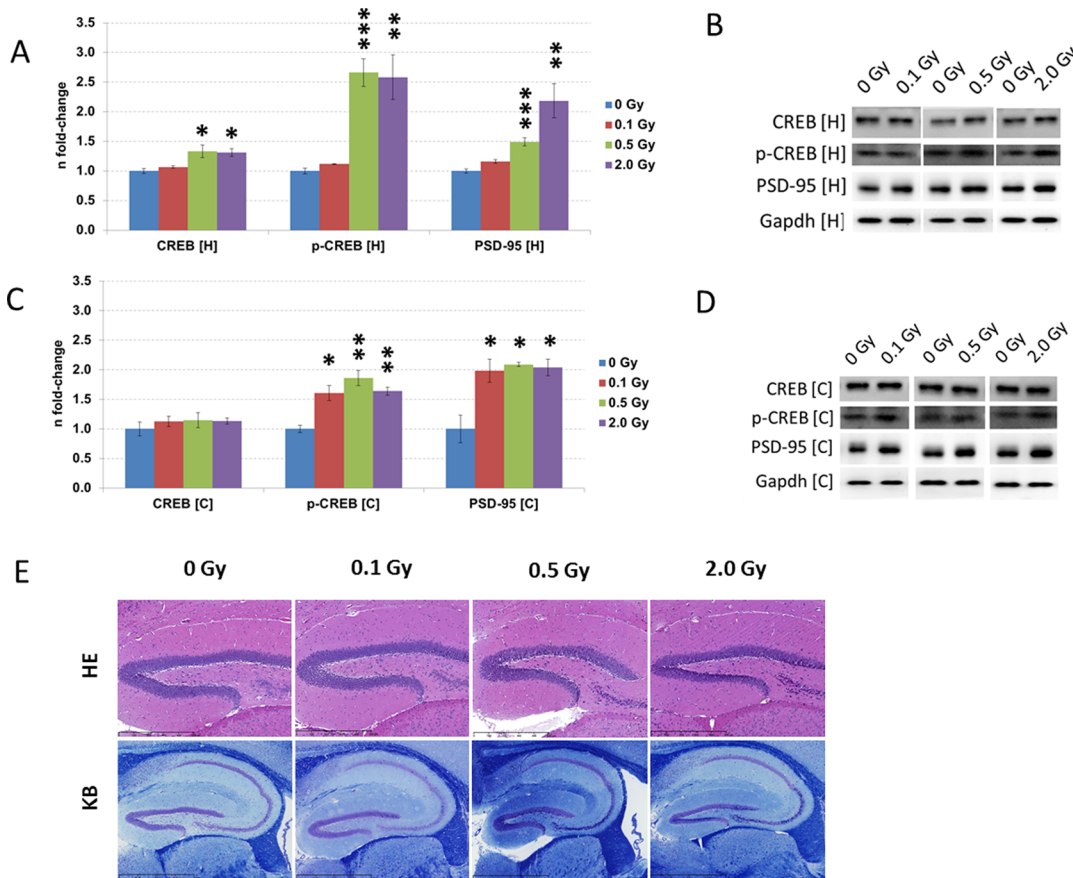


**Figure 4.** Immunoblotting of CREB, phospho-CREB, and PSD-95 in the hippocampus and cortex and hippocampal structure staining 24 weeks postirradiation. Data are shown from immunoblotting of proteins associated with LTD/LTP and CREB signaling pathways in cortex and hippocampus irradiated with 0 Gy, 0.1 Gy, 0.5 Gy, and 2.0 Gy 24 weeks postirradiation (A–D). The columns represent the fold-changes with standard errors of the mean (SEM);  $n = 3$ . \*,  $p < 0.05$ ; \*\*,  $p < 0.01$ ; \*\*\*,  $p < 0.001$  (unpaired Student's *t* test). Normalization was performed against endogenous GAPDH. Panel E shows the representative hippocampal staining with hematoxylin and eosin (HE) and Klüver Barrera (KB) to evaluate changes in brain morphology and demyelination processes, respectively, 24 weeks postirradiation (0 Gy, 0.1 Gy, 0.5 Gy, and 2.0 Gy). The staining was identically performed between all biological replicates ( $n = 6$ ). The light microscopic analysis was done independently by two experienced pathologists.

The radiation-induced proteome alterations in the isolated synaptosomes were analyzed. The complete list of deregulated synaptosomal proteins is shown in SI Tables S3 (cortex) and S4 (hippocampus). The protein quantification showed a large number of significantly deregulated proteins 5 weeks postirradiation (cortex/hippocampus: 0.1 Gy, 47/59 proteins; 0.5 Gy, 43/64 proteins; 2.0 Gy, 106/106 proteins) and 24 weeks postirradiation (cortex/hippocampus: 0.1 Gy, 73/40 proteins; 0.5 Gy, 91/84 proteins; 2.0 Gy, 152/168 proteins) (Figure 3A,B). A similar tendency was seen in the ratios of all affected proteins to all quantifiable proteins ( $\geq 2$  unique ICPL-labeled peptides found in  $n - 1$  runs) in the synaptosomes at 5 weeks (cortex/hippocampus: 0.1 Gy, 10.4%/11.1%; 0.5 Gy, 9.5%/12.1%; 2.0 Gy, 23.3%/20.2%) and 24 weeks postirradiation (cortex/hippocampus: 0.1 Gy, 13.0%/6.8%; 0.5 Gy, 15.7%/14.3%; 2.0 Gy, 27.0%/28.8%). Similar to whole cortex and hippocampus data (Figure 1A,B; SI Tables S1 and S2), annotation of the deregulated proteins into protein classes demonstrated that several proteins belonged to the protein class of cytoskeleton/cytoskeleton-associated proteins both in cortex and hippocampus (Figure 3A,B; SI Tables S3 and S4). Similar to the whole tissue proteomics, the level of Rac1 was also decreased in the synaptosomes (SI Tables S3 and S4). We also noted in the isolated synaptosomes an increase in the actin

cytoskeleton-organizing septin proteins (Sept3, 4, 5, and 7), several subunits of tubulin (Tubb's) and microtubule-associated proteins (Mtap's) as well as changes in the expression levels of proteins associated with neurofilaments (Nefl, Nefm) (SI Tables S3 and S4).

Pathway analysis (IPA) of all the deregulated proteins showed that the signaling pathways ephrin B/ephrin receptor signaling, signaling by Rho family GTPases, RhoGDI signaling, and axonal guidance signaling were persistently altered after radiation exposure at 0.5 and 2.0 Gy, especially in hippocampal synaptosomes (Figure 3C), while these signaling pathways were not significantly deregulated at 0.1 Gy dose (Figure 3C). This was in agreement with the proteomics data from the whole hippocampus and cortex (Figure 1C). The deregulated proteins at 0.1 Gy involved in cytoskeletal processes could not be assigned to synaptic signaling pathways (Figure 3A–C). IPA indicated a potential alteration in synaptic long-term potentiation/long-term depression (LTP/LTD) processes and CREB signaling at all doses and time points in the synaptosomes of both hippocampus and cortex (Figure 3D).

## Ionizing Radiation Targets the LTP-Mediated CREB Signaling Pathway

The phosphorylation status of CREB and the activation of LTP/LTD signaling are intertwined processes.<sup>36–38</sup> To further study these pathways, levels of total and phosphorylated CREB were quantified by immunoblotting from total hippocampal and cortical protein lysates at 24 weeks. The analysis showed that total CREB levels were only modestly elevated in the hippocampus at 0.5 and 2.0 Gy, while no alteration was found in the cortex (Figure 4A–D). In contrast, the levels of phosphorylated CREB were markedly increased in both the hippocampus (0.5 and 2.0 Gy) and cortex (all doses) (Figure 4A–D) suggesting an activation of the CREB signaling and LTP signaling<sup>38</sup> in both brain regions 24 weeks after irradiation. One of the CREB target genes is *Dlg4* gene coding for postsynaptic protein PSD-95.<sup>39</sup> That is consistent with our data showing increased PSD-95 levels in the hippocampus at 0.5 and 2.0 Gy and in the cortex at all doses (Figure 4A–D).

Since the level of PSD-95 plays an important role in synaptic plasticity and the stabilization of synaptic changes during LTP,<sup>40</sup> we quantified radiation-induced alterations in the expression of 84 genes involved in synaptic plasticity in cortex (2.0 Gy, 24 weeks). The expression of a number of genes involved in LTP-related synaptic plasticity was found to be increased. These genes encoded ephrin B2 (*Ephb2*), adenylate cyclase (*Adcy8*), postsynaptic neuronal glutamate receptors (*Gria4*, *Grin2a*, *Grin2c*, *Grm3* and *Grm4*), neuronal growth factors (*Igf1* and *Ngf*), and LTP-associated protein kinases (*Mapk*, *Prkca*, *Prkcc*, and *Prkg1*) (SI Table S5). Further, the activation of CREB due to its elevated phosphorylation status in the cortex (2.0 Gy) (Figure 4C,D) was reflected by enhanced transcription of the CREB target gene *Crem* (SI Table S5).<sup>41</sup> Although these proteins are not found in the list of dysregulated proteins probably due to their low abundance, the gene expression analysis confirms the involvement of LTP-related synaptic plasticity in the radiation-induced damage in the cortex indicated by the proteome analysis.

Importantly, ionizing radiation did not induce any obvious brain morphology changes as observed via HE staining or demyelination of the white matter via KB staining for myelin and Nissl bodies (Figure 4E).

## Long-Term Molecular Consequences of Ionizing Radiation in Cerebellum Are Similar to Those in Hippocampus and Cortex

The cerebellum plays an important role in motor control and may also be involved in some cognitive functions.<sup>42</sup> Therefore, a global proteomics analysis on the control and irradiated cerebellum and on cerebellar synaptosomes was performed. This showed similar alterations to signaling pathways as the hippocampus and cortex. Thus, we observed changes in the synaptic plasticity pathways (ephrin B signaling, signaling by Rho family GTPases, RhoGDI signaling, axonal guidance signaling, and ephrin receptor signaling) and LTP/LTD-related pathways (synaptic long-term depression/potentiation and CREB signaling in neurons) in the whole cerebellum (SI Figure S2A, SI Table S6) and cerebellar synaptosomes (SI Figure S2B, SI Table S7).

## Synaptic Mitochondria Are Affected in the Irradiated Brain

The proteome analysis of irradiated synaptosomes indicated that the signaling pathways associated with oxidative phosphorylation and mitochondrial dysfunction were significantly affected (Figure 5). Compared to the whole hippocampus and cortex, the importance of these pathways appeared to be concentrated in the synaptosomes. This was reflected by the large number of altered mitochondrial proteins in synaptosomes compared to the whole tissue. The mitochondrial proteins that were deregulated represented ATPases and all respiratory complexes except Complex II (SI Table S8). The number of deregulated synaptosomal mitochondrial proteins increased with time at doses of 0.5 Gy (cortex, 6 to 14; hippocampus, 6 to 13) and 2.0 Gy (cortex, 9 to 13; hippocampus, 12 to 24) but declined with time at 0.1 Gy (cortex, 7 to 2; hippocampus, 6 to 2) (SI Table S8). This could indicate persistent and progressive mitochondrial impairment at the higher radiation doses. The ATP synthases in the hippocampal synaptosomes appeared to be deregulated only at the later time point (24 weeks, 0.5 and 2.0 Gy) (SI Table S8).

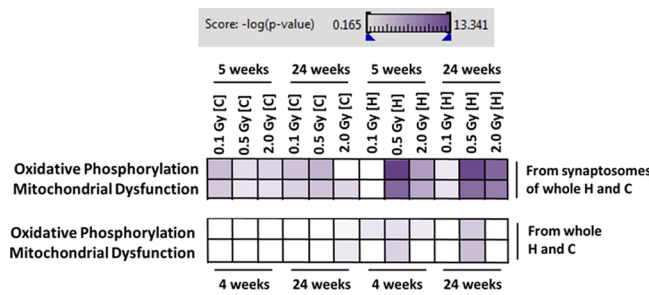


**Figure 5.** Mitochondria-associated pathways based on proteomics data in whole hippocampus and cortex and synaptosomes isolated from these tissues. Mitochondria-associated signaling pathways of oxidative phosphorylation and mitochondrial dysfunction of all deregulated proteins from hippocampal and cortical synaptosomes 5 weeks and 24 weeks postirradiation (upper panel) and from whole hippocampus and cortex 4 weeks and 24 weeks postirradiation (lower panel) using the IPA software. High color intensity represents high significance (*p*-value); all colored boxes have a *p*-value of  $\leq 0.05$ . Data from hippocampal and cortical synaptosomes result from three biological replicates where each biological replicate represents a pool of two independent samples; data from whole hippocampus and cortex correspond to six biological replicates; H, hippocampus, C, cortex.

campus and cortex, the importance of these pathways appeared to be concentrated in the synaptosomes. This was reflected by the large number of altered mitochondrial proteins in synaptosomes compared to the whole tissue. The mitochondrial proteins that were deregulated represented ATPases and all respiratory complexes except Complex II (SI Table S8). The number of deregulated synaptosomal mitochondrial proteins increased with time at doses of 0.5 Gy (cortex, 6 to 14; hippocampus, 6 to 13) and 2.0 Gy (cortex, 9 to 13; hippocampus, 12 to 24) but declined with time at 0.1 Gy (cortex, 7 to 2; hippocampus, 6 to 2) (SI Table S8). This could indicate persistent and progressive mitochondrial impairment at the higher radiation doses. The ATP synthases in the hippocampal synaptosomes appeared to be deregulated only at the later time point (24 weeks, 0.5 and 2.0 Gy) (SI Table S8).

## Mitochondria Isolated from Whole Hippocampus Show Dose-Dependent Reduction in Respiratory Capacity at 4 but Not at 24 Weeks

Mitochondria from the hippocampus were more sensitive to ionizing radiation than those from the cortex (Figure 5). Consequently, mitochondrial respiration was measured 4 and 24 weeks postirradiation using hippocampal mitochondria. This showed a dose-dependent reduction of OCR in mitochondrial respiration (Figure 6A), leading to significant reduction in states 3 and 4 respiration at 4 weeks (Figure 6B,C). In contrast to the changes in the proteome, this effect disappeared at 24 weeks (Figure 6D).

To investigate whether the hippocampal mitochondrial populations irradiated with different doses may differ in their molecular composition leading to discrepancies between protein concentration and mitochondrial number<sup>43</sup> and thus to an error in the respiration assay, we investigated the levels of citrate synthase as a measure of mitochondrial content.<sup>44</sup> No significant changes that could explain the restoration of the respiratory capacity were found in the level of citrate synthase in the proteomics analysis (SI Table S9).

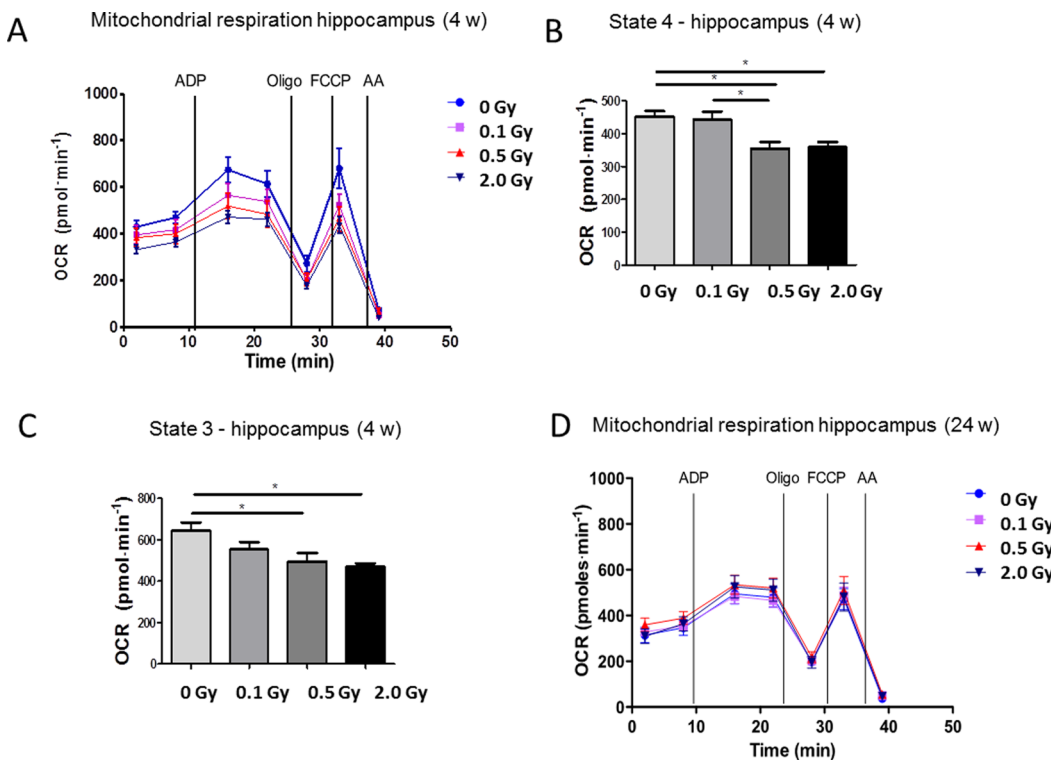


**Figure 6.** Mitochondrial respiration of total hippocampal mitochondria 4 and 24 weeks postirradiation. Total mitochondrial respiration was measured with a XF-24 Extracellular Flux Analyzer (Seahorse Bioscience) using 10  $\mu$ g of mitochondrial protein of irradiated hippocampi at (A) 4 weeks and (D) 24 weeks postirradiation using radiation doses of 0.1 Gy, 0.5 Gy, and 2.0 Gy. Respiration was sustained by succinate (10 mM) in the presence of rotenone. State 3 was elicited by addition of 4 mM ADP. Panels B and C show the statistical analysis of the states 4 and 3 respiration from the obtained data presented in panel A (4 weeks postirradiation), respectively. OCR, Oxygen consumption rate; FCCP, carbonyl cyanide-4-(trifluoromethoxy)phenylhydrazone; ADP, adenosine diphosphate; oligo: oligomycin; AA, antimycin A;  $n = 4$ ; \*,  $p < 0.05$  calculated by one-way ANOVA (Kruskal-Wallis test with Dunn's multiple comparison post-test). Error bars represent standard error of the mean (SEM).

## DISCUSSION

We have previously shown that exposure of neonatal male NMRI mice to external  $\gamma$  radiation results in persistent cognitive defects at the dose of 0.5 Gy and above but not at lower doses.<sup>17</sup> In an unpublished study on neonatal gamma exposure using C57Bl/6J male and female mice, behavioral defects were similar to those seen for NMRI mice (Per Eriksson, personal communication).<sup>17</sup> The aim of the present study was to see whether the biological mechanisms behind the radiation-induced cognitive effects are reproducible across different mouse strains and between genders. Since no gender-specific radiation effects have been observed in the cognition (Per Eriksson, personal communication), female mice were used in this study.

Some epidemiological studies indicate cognitive impairment in children even after doses around 0.1 Gy.<sup>4</sup> Therefore, we carefully investigated the long-term molecular effects of this radiation dose, although no effect on cognition has been observed at such low doses in NMRI<sup>17</sup> or C57Bl/6J mice.

### Irradiation Affects Synapse Morphology by Targeting the Rac1-Cofilin Pathway

The ability of dendritic spines to form synapses plays an important role in integrating and storing information.<sup>45</sup> Filamentous actin, the major cytoskeletal component in dendritic spines, is essential for maintaining the morphological integrity of synapses.<sup>46</sup> The morphological alterations in spinal cytoskeleton affecting shape, size, and number are dependent on local actin dynamics and signaling.<sup>47,48</sup> Our proteomics data

indicate alterations in abundance of cytoskeleton/cytoskeleton-associated proteins, particularly after radiation doses of 0.5 and 2.0 Gy. These alterations are found in both hippocampus and cortex as well as in synaptosomes isolated from these tissues. Signaling pathway analysis shows that, at 0.5 and 2.0 Gy but not at 0.1 Gy, proteins functionally involved in neuronal plasticity, formation, and strengthening of synapses, including ephrin b and ephrin receptor signaling components,<sup>49</sup> are altered. Ephrin signaling regulates axonal guidance maintenance, synaptic plasticity, and LTP during development and adulthood.<sup>50</sup> Moreover, proteins involved in signaling by RhoGDI and Rho family GTPases that also link to ephrin-induced processes<sup>51</sup> are deregulated only at these higher doses. These pathways share many proteins that all are members of the Rac1-Cofilin pathway, such as Rac1, PAK1/3, Cdc42, LIMK1, and cofilin. The persistently increased levels of total cofilin compared to that of phosphorylated inactive form are indicative of alterations in synaptic morphology processes by promoting actin depolymerization<sup>52</sup> and thus impairment in axonal outgrowth and elongation.<sup>52</sup> However, the changes in the levels of hippocampal Cdc42 and Rac1 seem to be involved only in the radiation-induced Rac1-Cofilin pathway regulation and are not associated with the myelin sheath formation<sup>53,54</sup> as we note no alteration in the myelination process.

The miRNAs miR-132 and miR-134 are important regulators of the Rac1-Cofilin pathway.<sup>34,35</sup> We observe increased expression of these miRNAs by up to two-fold in hippocampus and cortex after all radiation doses used in this study. Overexpression of miR-132 has been shown to impair short-

term recognition memory and attenuate LTD and LTP in the rat perirhinal cortex.<sup>55</sup>

The increased expression of the postsynaptic protein PSD-95 found in this study is in agreement with the results observed by Parikh and Limoli after cranial irradiation with doses of 1 and 10 Gy.<sup>56</sup> PSD-95 is involved in the development, outgrowth, branching, and maturation of dendritic spines and modulation of synaptic signals.<sup>57,58</sup> Elevated PSD-95 levels alter the ratio of excitatory to inhibitory synaptic contacts and thus neuronal excitability, a typical event in the pathobiology of several neurodegenerative diseases.<sup>59</sup> The increase of PSD-95 expression is likely to restrict the synaptic clustering of glutamatergic receptors and thereby reduce the level of dendritic branching.<sup>60</sup> This corroborates our suggestion for an altered balance of actin polymerization/depolymerization process that may persistently affect axonal outgrowth and dendritic spine formation.<sup>61</sup>

In general, the molecular alterations in the Rac1-Cofilin pathway and the level of PSD-95 correlate well with our previous data showing persistent downregulation of Rac1 but increased expression of miR-132, miR-134, and total cofilin in irradiated NMRI mice.<sup>17</sup> The decreased expression of Rac1 is also one of the early (24 h) hallmarks of ionizing radiation response both in mouse hippocampal neuronal HT22 cells and in hippocampus of NMRI mice.<sup>26</sup>

### Irradiation Enhances CREB Signaling

In this study, a persistent activation by radiation exposure of CREB signaling is observed, as evident from increased levels of phosphorylated CREB both in hippocampus and cortex, and enhanced expression of CREB target genes *Crem* and miR-132. Phosphorylation of CREB has been implicated in long-term synaptic plasticity and memory and is required for LTP maintenance.<sup>62</sup> Pharmacological elevation of CREB phosphorylation has been shown to ameliorate the memory impairment developing in mice irradiated acutely with 2.0 Gy.<sup>63</sup> It has also been shown as an immediate response to neonatal irradiation in the hippocampus of C57BL/6J mice.<sup>64</sup> However, the persistently increased phosphorylation of CREB in neonatally irradiated NMRI mice is clearly not enough to rescue the long-term radiation-induced impairment in cognition.<sup>17</sup> The increased phosphorylation of CREB may promote dendritegenesis and neuroprotection<sup>65</sup> that, however, is not able to fully compensate for the radiation damage.

### Ionizing Radiation Affects Cerebellar Signaling Pathways of Synaptic Integrity

The cerebellum has traditionally been characterized as a brain structure involved in motor coordination. However, recent studies using postnatally X-ray irradiated rats<sup>66</sup> and mice<sup>67</sup> show the involvement of cerebellum in cognitive tasks. Therefore, neonatal radiation exposure may induce cerebellar rearrangement accompanied by long-lasting spatial memory defects,<sup>68</sup> especially when taking into consideration that the cerebellum processes information in conjunction with the cerebral cortex.<sup>69</sup> In this study, the evaluation of radiation-induced long-term changes in the cerebellum using a proteomics approach indicates that synaptic plasticity and LTP/LTD-related pathways are affected in this part of the brain. The similarity of cerebellar proteomics observation to that of the irradiated hippocampus and cortex strongly suggests that alterations in cytoskeletal architecture of the synapse may also involve Rac1-Cofilin and CREB pathways.

### Ionizing Radiation Reduces Mitochondrial Functions

A proper functioning of synaptic mitochondria is necessary to sustain the high energy requirement that is necessary for loading of neurotransmitters in synaptic vesicles.<sup>70</sup> In our previous study using female neonatal C57BL/6J mice, we showed that signaling pathways related to mitochondrial functions were altered immediately (24 h postirradiation).<sup>64</sup> This occurred predominately in the cortex already at 0.1 Gy but in the hippocampus only at 0.5 Gy.<sup>64</sup> The present study shows that neonatal total body exposure to ionizing radiation significantly and persistently changes the mitochondrial proteome in the synaptosomes isolated from hippocampus and cortex. Increased number of deregulated mitochondrial proteins with time is clearly observed, indicating progression of the damage at doses equal to or above 0.5 Gy. In contrast, the changes in mitochondrial protein expression decline with time at the lowest dose (0.1 Gy) suggesting recovery.

In agreement with the mitochondrial proteome data, mitochondria isolated from the irradiated hippocampi show a dose-dependent reduction in state 3 and state 4 respiration at 0.5 and 2.0 Gy 4 weeks after the radiation exposure. The altered gene and protein expression levels of metabotropic G-protein-coupled glutamate receptors and changes in the Rac1-Cofilin pathway that are observed here may result in reduced axonal transport of synaptic mitochondria to the dendritic spines and synapses.<sup>71</sup> Primary neurons of APP $\beta$  mice (AD model) have been shown to have defects in axonal transport of mitochondria and mitochondrial biogenesis compared to wild-type neurons.<sup>72</sup>

The dose-dependent impairment in the mitochondrial respiration observed at 4 weeks disappeared at 24 weeks, but this cannot be explained by a radiation-induced discrepancy between protein concentration and mitochondrial number.<sup>43</sup> It has been known for some time that respiratory complexes associate to form functional supramolecular complexes. In the brain, Complexes I, III, and IV form at least partially I–III–IV and III–IV supercomplexes, which may be part of even larger respirasomes,<sup>73</sup> an association that provides kinetic advantage through substrate channeling.<sup>74</sup> Since the Complexes I, III, and IV are affected in their expression by ionizing radiation in this study, the supercomplex assembly may have emerged as a necessary step for restoration of the respiratory capacity. Until now, no studies are available concerning effects of ionizing radiation in the mitochondrial supercomplex formation, but further detailed investigations concerning this issue are in progress.

### CONCLUSION

This study provides evidence that long-term alterations in Rac1-Cofilin and CREB signaling pathways observed after neonatal irradiation are independent of mouse strain or gender. The changed expression and phosphorylation profiles of Rac1, cofilin, PSD-95, and CREB proteins form a molecular synaptic fingerprint that is typical for the radiation-induced damage to the brain at this developmental stage. This study also highlights the role of synaptosomal mitochondria as target molecules contributing to impairment in synaptic plasticity after radiation exposure. Importantly, the persistent radiation-induced effects are significant at doses of 0.5 Gy and above but not at a lower (0.1 Gy) dose. This limit to the observed changes is the same that has been seen with the cognition studies in mice. Although these data give no direct support to the linear no-threshold model on the effects of ionizing radiation in the brain, further

studies on mechanisms of cognitive and neurological dysfunction at low and moderate radiation doses are of critical importance in minimizing radiation-associated health risks.

## ■ ASSOCIATED CONTENT

### § Supporting Information

The Supporting Information is available free of charge on the ACS Publications website at DOI: [10.1021/acs.jproteome.5b00564](https://doi.org/10.1021/acs.jproteome.5b00564).

Distribution of protein markers in subcellular fractions from mouse hippocampus for characterization of synaptosomes enrichment quality using immunoblotting and mitochondrial respiration ([PDF](#))

Proteomics analysis of whole cerebellum at 4 and 24 weeks postirradiation and cerebellar synaptosomes from 5 and 24 weeks postirradiation ([PDF](#))

Deregulated proteins found in MS-based proteomics analysis in the whole cortex; deregulated proteins found in MS-based proteomics analysis in the whole hippocampus; deregulated proteins found in MS-based proteomics analysis in the isolated synaptosomes from whole cortex; deregulated proteins found in MS-based proteomics analysis in the isolated synaptosomes from whole hippocampus; pathway-focused transcriptome analysis of cortex; deregulated proteins found in MS-based proteomics analysis of the whole cerebellum; deregulated proteins found in MS-based proteomics analysis of the isolated synaptosomes from whole cerebellum; categorization of deregulated synaptosomal mitochondrial proteins isolated from hippocampus and cortex; expression levels of citrate synthase from proteomics analysis; complete list of antibodies used in this study ([XLS](#))

## ■ AUTHOR INFORMATION

### Corresponding Author

\*E-mail: [soile.tapio@helmholtz-muenchen.de](mailto:soile.tapio@helmholtz-muenchen.de). Phone: +49 89 3187 3445. Fax: +49 89 3187 3378.

### Present Address

<sup>†</sup>Department of Biochemistry and Molecular Biology, University of Southern Denmark, 5230 Odense, Denmark.

### Notes

The authors declare no competing financial interest.

## ■ ACKNOWLEDGMENTS

The research leading to these results was supported by a grant from the European Community's Seventh Framework Programme (EURATOM) Contract No. 29552 (CEREBRAD). The funders had no role in study design, data collection, analysis and interpretation, decision to publish, or preparation of the manuscript. We thank Stefanie Winkler, Sandra Helm, Martin Jastroch, and Maria Kutschke for their excellent technical assistance and Hans Zischka and Simone Mörtl for helpful discussions.

## ■ ABBREVIATIONS

AD, Alzheimer's disease; BSA, bovine serum albumin; CNS, central nervous system; CT, computed tomography; FDR, false discovery rate; IB, isolation buffer; OD, optical density; ICPL, isotope coded protein label; IPA, INGENUITY pathway

analysis; LTP, long-term potentiation; LTD, long-term depression; LC–MS, liquid chromatography–mass spectrometry; MS–MS, tandem mass spectrometry; OCR, oxygen consumption rate; PND10, postnatal day 10; PBS, phosphate-buffered saline; SAB, synaptosomal assay buffer; TES, N-[tris(hydroxymethyl)methyl]-2-aminoethanesulfonic acid

## ■ REFERENCES

- Bernier, M. O.; Rehel, J. L.; Brisse, H. J.; Wu-Zhou, X.; Caer-Lorho, S.; Jacob, S.; Chateil, J. F.; Aubert, B.; Laurier, D. Radiation exposure from CT in early childhood: a French large-scale multicentre study. *Br. J. Radiol.* **2012**, *85*, 53–60.
- Kim, J. S.; Yang, M.; Kim, S. H.; Shin, T.; Moon, C. Neurobiological toxicity of radiation in hippocampal cells. *Histol. Histopathol.* **2013**, *28*, 301–10.
- Li, J.; Bentzen, S. M.; Li, J.; Renschler, M.; Mehta, M. P. Relationship between neurocognitive function and quality of life after whole-brain radiotherapy in patients with brain metastasis. *Int. J. Radiat. Oncol., Biol., Phys.* **2008**, *71*, 64–70.
- Hall, P.; Adami, H. O.; Trichopoulos, D.; Pedersen, N. L.; Lagiou, P.; Ekbom, A.; Ingvar, M.; Lundell, M.; Granath, F. Effect of low doses of ionising radiation in infancy on cognitive function in adulthood: Swedish population based cohort study. *BMJ.* **2004**, *328*, 19.
- Ron, E.; Modan, B.; Floro, S.; Harkedar, I.; Gurewitz, R. Mental function following scalp irradiation during childhood. *Am. J. Epidemiol.* **1982**, *116*, 149–60.
- Pearce, M. S.; Salotti, J. A.; Little, M. P.; McHugh, K.; Lee, C.; Kim, K. P.; Howe, N. L.; Ronckers, C. M.; Rajaraman, P.; Sir Craft, A. W.; Parker, L.; Berrington de Gonzalez, A. Radiation exposure from CT scans in childhood and subsequent risk of leukaemia and brain tumours: a retrospective cohort study. *Lancet* **2012**, *380*, 499–505.
- Wiest, P. W.; Locken, J. A.; Heintz, P. H.; Mettler, F. A., Jr. CT scanning: a major source of radiation exposure. *Semin Ultrasound CT MR* **2002**, *23*, 402–10.
- UNSCEAR 2000. The United Nations Scientific Committee on the Effects of Atomic Radiation. *Health Phys.* **2000**, *79*, 314. [10.1097/00004032-200009000-00017](https://doi.org/10.1097/00004032-200009000-00017)
- Holland, B. A.; Haas, D. K.; Norman, D.; Brant-Zawadzki, M.; Newton, T. H. MRI of normal brain maturation. *AJNR Am. J. Neuroradiol.* **1986**, *7*, 201–8.
- Dobbing, J.; Sands, J. Comparative aspects of the brain growth spurt. *Early Hum. Dev.* **1979**, *3*, 79–83.
- Huttenlocher, P. R.; Dabholkar, A. S. Regional differences in synaptogenesis in human cerebral cortex. *J. Comp. Neurol.* **1997**, *387*, 167–78.
- Dekaban, A. S.; Sadowsky, D. Changes in brain weights during the span of human life: relation of brain weights to body heights and body weights. *Ann. Neurol.* **1978**, *4*, 345–56.
- Dobbing, J.; Sands, J. Quantitative growth and development of human brain. *Arch. Dis. Child.* **1973**, *48*, 757–67.
- Eriksson, P.; Ankarberg, E.; Fredriksson, A. Exposure to nicotine during a defined period in neonatal life induces permanent changes in brain nicotinic receptors and in behaviour of adult mice. *Brain Res.* **2000**, *853*, 41–8.
- Eriksson, P.; Fischer, C.; Stenerlow, B.; Fredriksson, A.; Sundell-Bergman, S. Interaction of gamma-radiation and methyl mercury during a critical phase of neonatal brain development in mice exacerbates developmental neurobehavioural effects. *NeuroToxicology* **2010**, *31*, 223–9.
- Zhu, C.; Huang, Z.; Gao, J.; Zhang, Y.; Wang, X.; Karlsson, N.; Li, Q.; Lannering, B.; Bjork-Eriksson, T.; Georg Kuhn, H.; Blomgren, K. Irradiation to the immature brain attenuates neurogenesis and exacerbates subsequent hypoxic-ischemic brain injury in the adult. *J. Neurochem.* **2009**, *111*, 1447–56.
- Kempf, S. J.; Casciati, A.; Buratovic, S.; Janik, D.; Toerne, C.; Ueffing, M.; Neff, F.; Moertl, S.; Stenerlow, B.; Saran, A.; Atkinson, M. J.; Eriksson, P.; Pazzaglia, S.; Tapio, S. The cognitive defects of neonatally irradiated mice are accompanied by changed synaptic

- plasticity, adult neurogenesis and neuroinflammation. *Mol. Neurodegener.* **2014**, *9*, 57.
- (18) Voloboueva, L. A.; Giffard, R. G. Inflammation, mitochondria, and the inhibition of adult neurogenesis. *J. Neurosci. Res.* **2011**, *89*, 1989–96.
- (19) Patrushev, M.; Kasymov, V.; Patrusheva, V.; Ushakova, T.; Gogvadze, V.; Gaziev, A. I. Release of mitochondrial DNA fragments from brain mitochondria of irradiated mice. *Mitochondrion* **2006**, *6*, 43–7.
- (20) Kempf, S. J.; Azimzadeh, O.; Atkinson, M. J.; Tapio, S. Long-term effects of ionising radiation on the brain: cause for concern? *Radiat. Environ. Biophys.* **2013**, *52*, 5–16.
- (21) Vos, M.; Lauwers, E.; Verstreken, P. Synaptic mitochondria in synaptic transmission and organization of vesicle pools in health and disease. *Front. Synaptic Neurosci.* **2010**, *2*, 139.
- (22) Cavallucci, V.; Nobili, A.; D'Amelio, M. Emerging role of mitochondria dysfunction in the onset of neurodegenerative diseases. *J. Biol. Regul. Homeost. Agents* **2013**, *27* (Suppl. 2), 1–9.
- (23) Eckert, A.; Nisbet, R.; Grimm, A.; Gotz, J. March separate, strike together—role of phosphorylated TAU in mitochondrial dysfunction in Alzheimer's disease. *Biochim. Biophys. Acta, Mol. Basis Dis.* **2014**, *1842*, 1258–66.
- (24) Kiebish, M. A.; Han, X.; Cheng, H.; Lunceford, A.; Clarke, C. F.; Moon, H.; Chuang, J. H.; Seyfried, T. N. Lipidomic analysis and electron transport chain activities in C57BL/6J mouse brain mitochondria. *J. Neurochem.* **2008**, *106*, 299–312.
- (25) Choi, S. W.; Gerencser, A. A.; Lee, D. W.; Rajagopalan, S.; Nicholls, D. G.; Andersen, J. K.; Brand, M. D. Intrinsic bioenergetic properties and stress sensitivity of dopaminergic synaptosomes. *J. Neurosci.* **2011**, *31*, 4524–34.
- (26) Kempf, S. J.; Buratovic, S.; von Toerne, C.; Moerth, S.; Stenerlow, B.; Hauck, S. M.; Atkinson, M. J.; Eriksson, P.; Tapio, S. Ionising radiation immediately impairs synaptic plasticity-associated cytoskeletal signalling pathways in HT22 cells and in mouse brain: an in vitro/in vivo comparison study. *PLoS One* **2014**, *9*, e110464.
- (27) Merl, J.; Ueffing, M.; Hauck, S. M.; von Toerne, C. Direct comparison of MS-based label-free and SILAC quantitative proteome profiling strategies in primary retinal Muller cells. *Proteomics* **2012**, *12*, 1902–11.
- (28) Shaltiel, G.; Hanan, M.; Wolf, Y.; Barbash, S.; Kovalev, E.; Shoham, S.; Soreq, H. Hippocampal microRNA-132 mediates stress-inducible cognitive deficits through its acetylcholinesterase target. *Brain Struct. Funct.* **2013**, *218*, 59–72.
- (29) Tanori, M.; Pasquali, E.; Leonardi, S.; Casciati, A.; Giardullo, P.; De Stefano, I.; Mancuso, M.; Saran, A.; Pazzaglia, S. Developmental and oncogenic radiation effects on neural stem cells and their differentiating progeny in mouse cerebellum. *Stem Cells* **2013**, *31*, 2506–16.
- (30) Saneyoshi, T.; Fortin, D. A.; Soderling, T. R. Regulation of spine and synapse formation by activity-dependent intracellular signaling pathways. *Curr. Opin. Neurobiol.* **2010**, *20*, 108–15.
- (31) Martinez, L. A.; Tejada-Simon, M. V. Pharmacological inactivation of the small GTPase Rac1 impairs long-term plasticity in the mouse hippocampus. *Neuropharmacology* **2011**, *61*, 305–12.
- (32) Kuhn, T. B.; Meberg, P. J.; Brown, M. D.; Bernstein, B. W.; Minamide, L. S.; Jensen, J. R.; Okada, K.; Soda, E. A.; Bamburg, J. R. Regulating actin dynamics in neuronal growth cones by ADF/cofilin and rho family GTPases. *J. Neurobiol.* **2000**, *44*, 126–44.
- (33) Magill, S. T.; Cambronne, X. A.; Luikart, B. W.; Lioy, D. T.; Leighton, B. H.; Westbrook, G. L.; Mandel, G.; Goodman, R. H. microRNA-132 regulates dendritic growth and arborization of newborn neurons in the adult hippocampus. *Proc. Natl. Acad. Sci. U. S. A.* **2010**, *107*, 20382–7.
- (34) Impey, S.; Davare, M.; Lasiek, A.; Fortin, D.; Ando, H.; Varlamova, O.; Obrietan, K.; Soderling, T. R.; Goodman, R. H.; Wayman, G. A. An activity-induced microRNA controls dendritic spine formation by regulating Rac1-PAK signaling. *Mol. Cell. Neurosci.* **2010**, *43*, 146–56.
- (35) Schrott, G. M.; Tuebing, F.; Nigh, E. A.; Kane, C. G.; Sabatini, M. E.; Kiebler, M.; Greenberg, M. E. A brain-specific microRNA regulates dendritic spine development. *Nature* **2006**, *439*, 283–9.
- (36) Ying, S. W.; Futter, M.; Rosenblum, K.; Webber, M. J.; Hunt, S. P.; Bliss, T. V.; Bramham, C. R. Brain-derived neurotrophic factor induces long-term potentiation in intact adult hippocampus: requirement for ERK activation coupled to CREB and upregulation of Arc synthesis. *J. Neurosci.* **2002**, *22*, 1532–40.
- (37) Cao, H.; Cui, Y. H.; Zhao, Z. Q.; Cao, X. H.; Zhang, Y. Q. Activation of extracellular signal-regulated kinase in the anterior cingulate cortex contributes to the induction of long-term potentiation in rats. *Neurosci. Bull.* **2009**, *25*, 301–8.
- (38) Paul, C.; Stratal, C.; Hofmann, F.; Kleppisch, T. cGMP-dependent protein kinase type I promotes CREB/CRE-mediated gene expression in neurons of the lateral amygdala. *Neurosci. Lett.* **2010**, *473*, 82–6.
- (39) Wang, Z.; Yan, P.; Hui, T.; Zhang, J. Epigenetic upregulation of PSD-95 contributes to the rewarding behavior by morphine conditioning. *Eur. J. Pharmacol.* **2014**, *732*, 123–9.
- (40) Meyer, D.; Bonhoeffer, T.; Scheuss, V. Balance and stability of synaptic structures during synaptic plasticity. *Neuron* **2014**, *82*, 430–43.
- (41) Kadar, E.; Huguet, G.; Aldavert-Vera, L.; Morgado-Bernal, I.; Segura-Torres, P. Intracranial self stimulation upregulates the expression of synaptic plasticity related genes and Arc protein expression in rat hippocampus. *Genes Brain Behav* **2013**, *12*, 771–9.
- (42) Wolf, U.; Rapoport, M. J.; Schweizer, T. A. Evaluating the affective component of the cerebellar cognitive affective syndrome. *J. Neuropsychiatry Clin. Neurosci.* **2009**, *21*, 245–53.
- (43) Schmitt, S.; Schulz, S.; Schropp, E. M.; Eberhagen, C.; Simmons, A.; Beisker, W.; Aichler, M.; Zischka, H. Why to compare absolute numbers of mitochondria. *Mitochondrion* **2014**, *19*, 113–23.
- (44) Bishop, D. J.; Granata, C.; Eynon, N. Can we optimize the exercise training prescription to maximise improvements in mitochondria function and content? *Biochim. Biophys. Acta, Gen. Subj.* **2014**, *1840*, 1266–75.
- (45) Kasai, H.; Matsuzaki, M.; Noguchi, J.; Yasumatsu, N.; Nakahara, H. Structure-stability-function relationships of dendritic spines. *Trends Neurosci.* **2003**, *26*, 360–8.
- (46) Urbanska, M.; Swiech, L.; Jaworski, J. Developmental plasticity of the dendritic compartment: focus on the cytoskeleton. *Adv. Exp. Med. Biol.* **2012**, *970*, 265–84.
- (47) Cohen, R. S.; Chung, S. K.; Pfaff, D. W. Immunocytochemical localization of actin in dendritic spines of the cerebral cortex using colloidal gold as a probe. *Cell. Mol. Neurobiol.* **1985**, *5*, 271–84.
- (48) Fifkova, E.; Delay, R. J. Cytoplasmic actin in neuronal processes as a possible mediator of synaptic plasticity. *J. Cell Biol.* **1982**, *95*, 345–50.
- (49) Sloniowski, S.; Ethell, I. M. Looking forward to EphB signaling in synapses. *Semin. Cell Dev. Biol.* **2012**, *23*, 75–82.
- (50) Kullander, K.; Klein, R. Mechanisms and functions of Eph and ephrin signalling. *Nat. Rev. Mol. Cell Biol.* **2002**, *3*, 475–86.
- (51) Nishida, H.; Okabe, S. Direct astrocytic contacts regulate local maturation of dendritic spines. *J. Neurosci.* **2007**, *27*, 331–40.
- (52) Lisman, J. Actin's actions in LTP-induced synapse growth. *Neuron* **2003**, *38*, 361–2.
- (53) Guo, L.; Moon, C.; Zheng, Y.; Ratner, N. Cdc42 Regulates Schwann Cell Radial Sorting and Myelin Sheath Folding Through NF2/Merlin-Dependent and Independent Signaling. *Glia* **2013**, *61*, 1906–1921.
- (54) Benninger, Y.; Thurnherr, T.; Pereira, J. A.; Krause, S.; Wu, X.; Chrostek-Grashoff, A.; Herzog, D.; Nave, K.-A.; Franklin, R. J. M.; Meijer, D.; Brakebusch, C.; Suter, U.; Relvas, J. B. Essential and distinct roles for cdc42 and rac1 in the regulation of Schwann cell biology during peripheral nervous system development. *J. Cell Biol.* **2007**, *177*, 1051–1061.
- (55) Scott, H. L.; Tamagnini, F.; Narduzzo, K. E.; Howarth, J. L.; Lee, Y. B.; Wong, L. F.; Brown, M. W.; Warburton, E. C.; Bashir, Z. I.;

- Uney, J. B. MicroRNA-132 regulates recognition memory and synaptic plasticity in the perirhinal cortex. *Eur. J. Neurosci.* **2012**, *36*, 2941–8.
- (56) Parihar, V. K.; Limoli, C. L. Cranial irradiation compromises neuronal architecture in the hippocampus. *Proc. Natl. Acad. Sci. U. S. A.* **2013**, *110*, 12822–7.
- (57) Chen, Y.; Rex, C. S.; Rice, C. J.; Dube, C. M.; Gall, C. M.; Lynch, G.; Baram, T. Z. Correlated memory defects and hippocampal dendritic spine loss after acute stress involve corticotropin-releasing hormone signaling. *Proc. Natl. Acad. Sci. U. S. A.* **2010**, *107*, 13123–8.
- (58) Matsuzaki, M.; Honkura, N.; Ellis-Davies, G. C.; Kasai, H. Structural basis of long-term potentiation in single dendritic spines. *Nature* **2004**, *429*, 761–6.
- (59) Levinson, J. N.; Chery, N.; Huang, K.; Wong, T. P.; Gerrow, K.; Kang, R.; Prange, O.; Wang, Y. T.; El-Husseini, A. Neuroligins mediate excitatory and inhibitory synapse formation: involvement of PSD-95 and neurexin-1beta in neuroligin-induced synaptic specificity. *J. Biol. Chem.* **2005**, *280*, 17312–9.
- (60) Bustos, F. J.; Varela-Nallar, L.; Campos, M.; Henriquez, B.; Phillips, M.; Opazo, C.; Aguayo, L. G.; Montecino, M.; Constantine-Paton, M.; Inestrosa, N. C.; van Zundert, B. PSD95 suppresses dendritic arbor development in mature hippocampal neurons by occluding the clustering of NR2B-NMDA receptors. *PLoS One* **2014**, *9*, e94037.
- (61) Cameron, H. A.; McKay, R. D. Adult neurogenesis produces a large pool of new granule cells in the dentate gyrus. *J. Comp. Neurol.* **2001**, *435*, 406–17.
- (62) Leutgeb, J. K.; Frey, J. U.; Behnisch, T. Single cell analysis of activity-dependent cyclic AMP-responsive element-binding protein phosphorylation during long-lasting long-term potentiation in area CA1 of mature rat hippocampal-organotypic cultures. *Neuroscience* **2005**, *131*, 601–10.
- (63) Kim, J. S.; Yang, M.; Cho, J.; Kim, S. H.; Kim, J. C.; Shin, T.; Moon, C. Promotion of cAMP responsive element-binding protein activity ameliorates radiation-induced suppression of hippocampal neurogenesis in adult mice. *Toxicol. Res.* **2010**, *26*, 177–83.
- (64) Kempf, S. J.; Moertl, S.; Sepe, S.; von Toerne, C.; Hauck, S. M.; Atkinson, M. J.; Mastroberardino, P. G.; Tapio, S. Low-dose ionizing radiation rapidly affects mitochondrial and synaptic signaling pathways in murine hippocampus and cortex. *J. Proteome Res.* **2015**, *14*, 2055–64.
- (65) Sakamoto, K.; Karelina, K.; Obrietan, K. CREB: a multifaceted regulator of neuronal plasticity and protection. *J. Neurochem.* **2011**, *116*, 1–9.
- (66) Le Marec, N.; Dahhaoui, M.; Stelz, T.; Bakalian, A.; Delhay-Bouchaud, N.; Caston, J.; Mariani, J. Effect of cerebellar granule cell depletion on spatial learning and memory and in an avoidance conditioning task: studies in postnatally X-irradiated rats. *Dev. Brain Res.* **1997**, *99*, 20–8.
- (67) Manda, K.; Ueno, M.; Anzai, K. Memory impairment, oxidative damage and apoptosis induced by space radiation: ameliorative potential of alpha-lipoic acid. *Behav. Brain Res.* **2008**, *187*, 387–95.
- (68) Caceres, L. G.; Rios, H.; Guelman, L. R. Long-lasting effects of neonatal ionizing radiation exposure on spatial memory and anxiety-like behavior. *Ecotoxicol. Environ. Saf.* **2009**, *72*, 895–904.
- (69) Colombel, C.; Lalonde, R.; Caston, J. The effects of unilateral removal of the cerebellar hemispheres on spatial learning and memory in rats. *Brain Res.* **2004**, *1004*, 108–15.
- (70) Saxton, W. M.; Hollenbeck, P. J. The axonal transport of mitochondria. *J. Cell Sci.* **2012**, *125*, 2095–104.
- (71) DuBoff, B.; Feany, M.; Gotz, J. Why size matters - balancing mitochondrial dynamics in Alzheimer's disease. *Trends Neurosci.* **2013**, *36*, 325–35.
- (72) Calkins, M. J.; Manczak, M.; Mao, P.; Shirendeb, U.; Reddy, P. H. Impaired mitochondrial biogenesis, defective axonal transport of mitochondria, abnormal mitochondrial dynamics and synaptic degeneration in a mouse model of Alzheimer's disease. *Hum. Mol. Genet.* **2011**, *20*, 4515–29.
- (73) Dencher, N. A.; Frenzel, M.; Reifschneider, N. H.; Sugawa, M.; Krause, F. Proteome alterations in rat mitochondria caused by aging. *Ann. N. Y. Acad. Sci.* **2007**, *1100*, 291–8.
- (74) Genova, M. L.; Lenaz, G. Functional role of mitochondrial respiratory supercomplexes. *Biochim. Biophys. Acta, Bioenerg.* **2014**, *1837*, 427–43.